

# Probing lattice vibration at surface and interface of SiO<sub>2</sub>/Si with nanometer resolution

Yuehui Li<sup>1,2</sup>, Mei Wu<sup>1</sup>, Ning Li<sup>1,2</sup>, Yuanwei Sun<sup>1,2</sup>, Chenglong Shi<sup>3</sup>, Xuetao Zhu<sup>4</sup>, Jiandong Guo<sup>4</sup>, Dapeng Yu<sup>2,5,6</sup>, Peng Gao<sup>1,2,6\*</sup>

<sup>1</sup>International Center for Quantum Materials, Peking University, Beijing, 100871, China

<sup>2</sup>Electron Microscopy Laboratory, School of Physics, Peking University, Beijing, 100871, China

<sup>3</sup>Nion Company, 11511 NE 118Th Street, Kirkland, Washington State, 98034, USA

<sup>4</sup>Beijing National Laboratory for Condensed Matter Physics and Institute of Physics, Chinese Academy of Sciences, Beijing 100190, China

<sup>5</sup>Shenzhen Key Laboratory of Quantum Science and Engineering, Shenzhen 518055, China

<sup>6</sup>Collaborative Innovation Centre of Quantum Matter, Beijing 100871, China.

Y.H.L. and M.W. contributed equally to this work.

E-mails: [p-gao@pku.edu.cn](mailto:p-gao@pku.edu.cn)

**Abstract:** Recent advances in monochromatic aberration corrected electron microscopy make it possible to detect the lattice vibration with both high-energy resolution (sub 10 meV) and high spatial resolution ( $\sim 0.1$  nm). Here we use this technique to investigate vibrational properties at surface and interface of an amorphous SiO<sub>2</sub> (a-SiO<sub>2</sub>) film on Si substrate. With  $\sim 8$  meV energy resolution, three optical vibration modes are simultaneously recorded and subtle energy shift between bulk and surface modes can be distinguished. We find that these vibration modes have different sensitivity of energy and intensity to the surface, thickness and interface. Particularly, the vibration energy of surface modes is lower than that of the corresponding bulk modes and shows a red-shift as z-thickness (parallel to fast electron beam) of SiO<sub>2</sub> film decreases due to the coupling of upper and lower surfaces, while the energy of bulk mode remains unchanged. In the vacuum, different surface modes have different decay behavior of intensity, while inside the SiO<sub>2</sub>, the intensity of bulk modes linearly increases with thickness

being increased. Approaching the SiO<sub>2</sub>/Si interface, the vibration energy remains almost unchanged but the vibration intensity drops steeply to zero within a few nanometers near the interface. Furthermore, the vibrational signal of Si substrate is not detected due to the retardation effects. The mechanism of the observed dependence is discussed and quantitatively compared with dielectric response theory analysis. Our nanometer scale measurements of vibrations properties provide useful information about the bonding conditions at the surface and interface and thus may help to design better silicon-based electronic devices via surface and interface treatments.

**Key words:** vibrational EELS; scanning transmission electron microscopy; surface; interface; dielectric theory

## **Introduction**

Lattice vibrations play a major role in many of the physical properties of condensed matter, including thermal (e.g. specific heat, thermal conductivity, and phase transition), electrical (e.g. electrical conductivity, superconductivity), and optical (e.g. polaritons, photonic, negative refraction) properties[1]. Measurements of vibration properties are vital to analyze the chemical bonding, isotope information, defect density, and strain state. At the surface and interface of solid materials, the change of atomic bonding state is expected to alter the local vibration behavior (such as phonon softening[2]), which should influence the localized physical properties via various phonon interactions (e.g. phonon-photon, phonon-electron, phonon-phonon). Therefore, exploring the localized vibration behavior is of significant importance. Particularly for the low dimensional materials in which the effects of surface and interface become more pronounced, the localized vibration properties may dominate the entire response of devices[3,4].

The vibrational properties are commonly measured by high-resolution electron energy loss spectroscopy (HREELS)[5,6], inelastic neutron scattering, infrared spectroscopy (IR)[7,8], and Raman spectroscopy[9]. The spatial resolution of these techniques, however, is typically at micrometer-scale (unless assisted by a sharp metal tip, e.g. tip enhanced Raman

spectroscopy[10], ~20nm), and thus it is not convenient to extract the local vibration properties. On the other hand, the tip-enhanced techniques based on surface probe are inaccessible to the vibrational properties of the buried interface. In contrast, the recent advancements of dedicated scanning transmission electron microscope with aberration corrector and monochromatic cold field emission gun enable an electron probe with ~10 meV in energy resolution and ~0.1 nm in spatial resolution, allowing us directly map the phonon structure of a single nanostructure[11–19], which provides an unprecedented opportunity to study the localized vibration properties of surface and interface.

In this paper, we use ~8 meV electron probe based on Nion UltraSTEM™ 200 microscope to study the vibrational properties of SiO<sub>2</sub>/Si heterostructure. SiO<sub>2</sub> film is commonly used as the gate dielectric material in metal-oxide-semiconductor field effect transistors (MOSFETs). The quality and properties of the SiO<sub>2</sub> films and the SiO<sub>2</sub>/Si interface can significantly influence the performance and stability of MOSFET's and bipolar transistors used in the integrated circuits[20,21]. The nanoscale structure and properties of the SiO<sub>2</sub>/Si interface becomes more and more important as the device size drops to tens of nanometer or lower[22]. For example, previously IR spectroscopy showed that purely geometrical effects result in substantial red-shifts of the transverse-optical (TO) mode while no obvious thickness dependence for the longitudinal (LO) mode for slab thickness ranging from 1000 nm to 10 nm[23,24]. The recent electron microscopy studies[11,13] provided more valuable insights into the decay distance of some aloof modes and intensity change at the boundary. However, the limited energy resolution in these studies (typically ~16 meV) was not sufficient to distinguish the surface and bulk modes and thus the mode-dependent vibration behavior at the surface and interface is still largely unknown.

In our study, we improve the energy resolution up to ~8 meV at 60 kV, which allows us not only simultaneously acquire three different vibration modes [i.e., TO<sub>1</sub> (~60 meV), TO<sub>2</sub> (~103 meV), TO<sub>3</sub> (~130meV–150meV)], but also capture the subtle changes of vibration energy and intensity at the surface and interface of SiO<sub>2</sub> film on Si substrate. We find that these vibration modes exhibit different behavior to the surface, thickness and interface. The surface modes

have lower energy than the corresponding bulk modes. As  $z$ -thickness decreases ( $z$  denotes the electron propagation direction), the vibration energy of  $TO_3$  mode shows a substantial red-shift but the  $TO_1$  surface mode only shows a subtle shift, while the energy of all the three bulk modes remain unchanged. The red-shift of surface mode is attributed to the enhanced coupling of upper and lower surfaces[25]. The maximum intensity of surface modes occurs at the surface edge and different modes have different decay distance. The vibration intensity of bulk modes is proportional to the slab thickness. The vibrational signal of Si substrate, however, is not detected due to the retardation effects. These results can be qualitatively interpreted by a semiclassical relativistic local dielectric model[25,26]. Our study reveals the vibration behavior of  $SiO_2$  at the surface and interface with nanometer resolution, providing useful insights into understanding the fundamental electrical, optical and thermal properties of surface and interface of  $SiO_2$ .

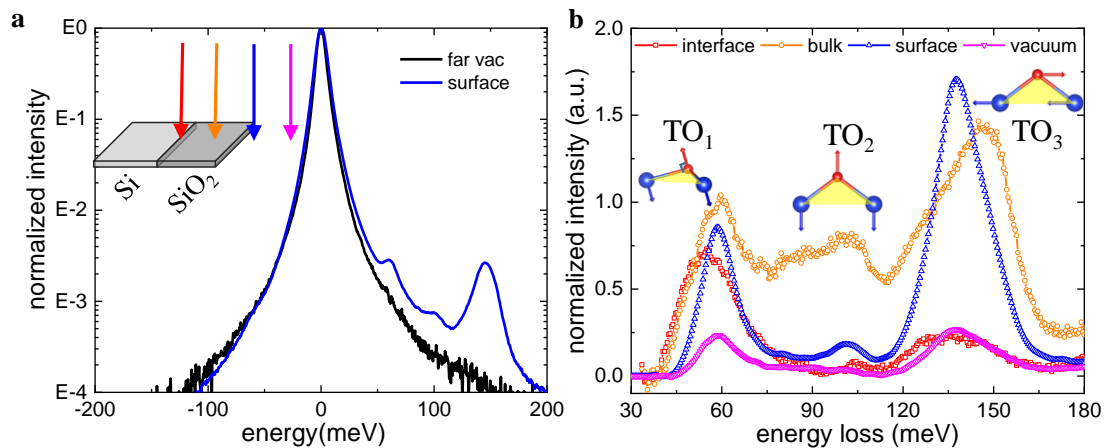


Fig 1. Electron energy loss spectroscopy measurement of  $SiO_2$  vibration modes in a monochromatic aberration corrected electron microscope. (a) Normalized spectra acquired with an electron beam located in vacuum side (blue) and vacuum (black) far away from specimen. The inset shows four different  $TO$  regions to record the spectra. (b) Typical spectra acquired from different regions: red, beam located in Si near the interface of  $SiO_2/Si$ ; orange, beam located in bulk  $SiO_2$ ; blue, beam located in vacuum near surface; pink, beam located in vacuum. The insets show the schematic representation of the three optical vibrational motions, the orange region shows the Si-O-Si plane. For the  $TO_1$  mode, rocking motion perpendicular to Si-O-Si plane;  $TO_2$  mode, symmetric stretching motion along the bisector of the Si-O-Si bridging angle;  $TO_3$  mode, antisymmetric stretching motion parallel to the Si-Si line between the two bridged cations.

## Results and discussion

A  $\sim 6$  meV zero-loss peak can be tuned up at 60 kV (Supporting Fig S1). For a higher ratio of signal to noise, we significantly increase the acquisition time in practical measurements which only sacrifices the energy resolution slightly. Fig 1a shows the typical measured EELS spectra with a probe beam located near surface in vacuum side (blue) and vacuum far away from specimen (black) where no vibration signal is detected. The energy resolution in Fig 1a is  $\sim 8$  meV, which is high enough to obtain the details of vibration spectra for the  $\text{SiO}_2$ . After background subtraction, the spectra in Fig 1b shows three peaks which are in agreement with previous IR spectroscopy and neutron scattering experiment[27,28]. For each spectrum, three vibration modes can be obtained, labeled as  $\text{TO}_1$  ( $\sim 60$  meV),  $\text{TO}_2$  ( $\sim 103$  meV),  $\text{TO}_3$  ( $\sim 130$ - $150$  meV), where  $\text{TO}_1$  mode is associated with Si-O-Si rocking motions, with bridging oxygen moving perpendicular to the Si-O-Si plane;  $\text{TO}_2$  mode is assigned to transverse-optical stretching motions, with oxygen atoms moving along a line bisecting the Si-O-Si bond;  $\text{TO}_3$  mode is associated with Si-O-Si antisymmetric stretching motion, with oxygen atoms moving along a line parallel to the Si-Si axis; as shown in Fig 1b (see also Supporting Fig S2 for details)[28]. Interestingly, the spatially resolved spectra exhibit these modes have different energy and intensity at different regions, indicating the vibration properties are sensitive to the surface and interface, with the details discussed below.

We first investigate the surface effect on the vibrational spectra. Fig 2a shows a high angle annular dark field (HAADF) image of an a- $\text{SiO}_2$  film with thickness of  $\sim 300$  nm on Si substrate. Fig 2b is the corresponding EELS mapping in which the surface position is set to zero, the negative distance denotes that the electron beam is in the vacuum and positive distance denotes that the electron beam is positioned inside the a- $\text{SiO}_2$  film. The  $\text{TO}_1$  mode and  $\text{TO}_3$  mode can spread over  $\sim 600$  nm in the vacuum, while the  $\text{TO}_2$  mode only concentrates near the surface. In Fig 2c, the selected line profiles of spectra recorded from the vacuum to a- $\text{SiO}_2$  with 6.3 nm every step displays the peak of  $\text{TO}_3$  mode in an a- $\text{SiO}_2$  region becomes broad and shifts to higher energy, suggesting the possible co-existence of two vibration modes with different energy in the film. In fact, this is because when placing probing beam inside the

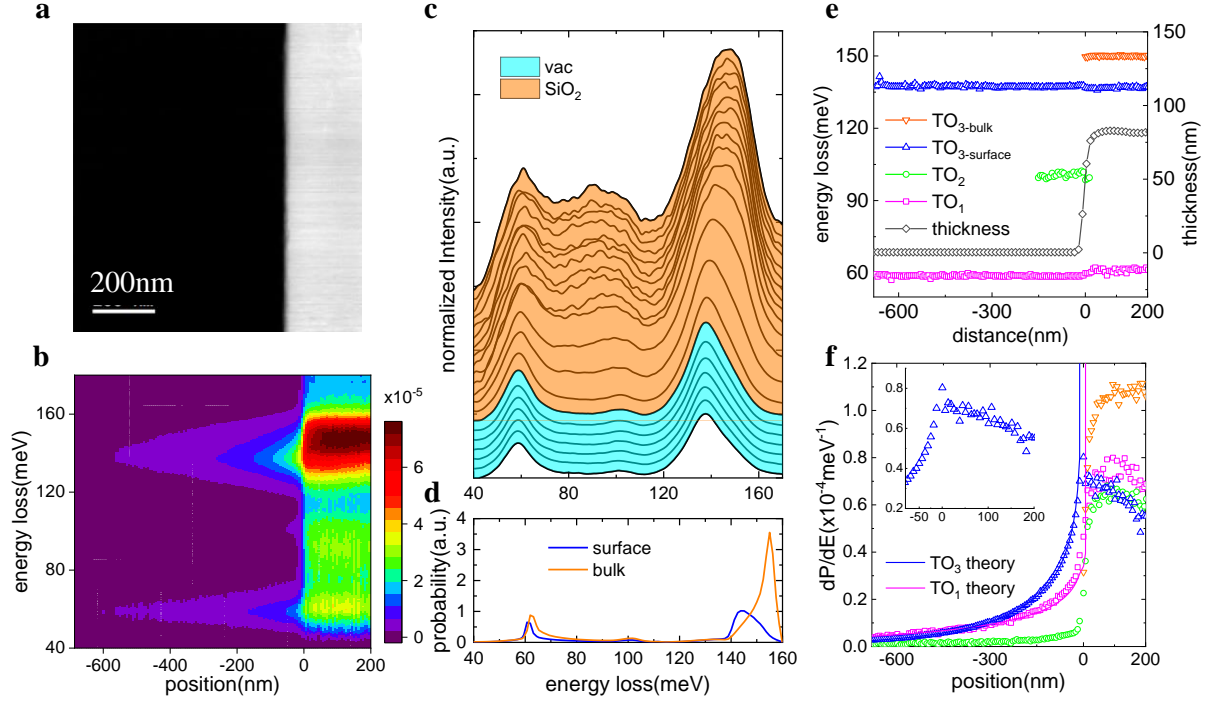


Fig 2. Vibrational energy and intensity of SiO<sub>2</sub> surface. (a) HAADF image of vacuum/a-SiO<sub>2</sub>/Si specimen viewed in cross-section. (b) Two dimensional plots of normalized intensity for beam located in different region. The surface position is labeled as zero, and negative distance denotes that the electron beam is in vacuum while positive distance denotes that the electron beam positioned within the SiO<sub>2</sub>. Color represents the normalized intensity. (c) Selected line profiles of the SiO<sub>2</sub> vibrational signal with 6.3 nm every stack. Orange region, beam located in SiO<sub>2</sub>; cyan region, beam located in vacuum. (d) Energy-loss functions of surface and SiO<sub>2</sub>,  $Im(-1/(1 + \epsilon_{SiO_2}(E)))$  and  $Im(-1/\epsilon_{SiO_2}(E))$ , respectively. (e) Vibration energy (colored) of different modes, and z-thickness (black) of SiO<sub>2</sub> slab are plotted as a function of the probe position. (f) Vibration intensity as a function of the probe position. Solid line represents theory calculation.

a-SiO<sub>2</sub> the surface mode (originates from upper and lower surfaces) and the bulk mode are mixed together due to the small difference in energy, broadening the TO<sub>3</sub> peak. The energy difference between the surface and the bulk modes can be interpreted by the energy loss function of surface vibration and bulk vibration,  $Im(-1/(1 + \epsilon_{SiO_2}(E)))$  and  $Im(-1/\epsilon_{SiO_2}(E))$ , respectively, as shown in Fig 2d. To extract the details of the bulk and surface modes, by using Gaussian functions (see Supporting Fig S3 for details) we decompose the signal in 120meV~170meV into two peaks, i.e., TO<sub>3-surface</sub> and TO<sub>3-bulk</sub>, which represent the surface and bulk modes, respectively. For the TO<sub>1</sub> mode, the difference between bulk and

surface modes is subtle (about 3 meV larger in SiO<sub>2</sub> than that in vacuum) which is also consistent with analysis of energy loss functions, while for the TO<sub>2</sub> mode, the significant broadening makes it hard to identify the peak positions in the SiO<sub>2</sub>.

The energy of four vibration modes (TO<sub>1</sub>, TO<sub>2</sub>, TO<sub>3-surface</sub>, TO<sub>3-bulk</sub>) as well as the film thickness (see Supporting Fig S4 for calculation details) are plotted in Fig 2e. Note that the energy of bulk modes doesn't change. When the electron beam is positioned at surface, the vibration energy of TO<sub>1</sub>, TO<sub>2</sub>, TO<sub>3-surface</sub>, TO<sub>3-bulk</sub> modes are 59 meV, 100 meV, 137 meV, 150meV respectively. The energies of TO<sub>1</sub>, TO<sub>2</sub> modes are in agreement with the calculation results: 60.5 meV for TO<sub>1</sub> and 100.4 meV for TO<sub>2</sub>. However, the simulated energy of TO<sub>3-surface</sub> mode in Fig 2d is 143 meV that is considerably larger than the measured value of 137 meV. The difference may be caused by the infinite slab thickness assumption calculation used in the calculations based on infinite mode while the practical thickness of SiO<sub>2</sub> slab is finite, i.e. ~83 nm as shown in Fig 2e (black line). It should be noted that the TO<sub>2</sub> mode 'disappears' when the probe is ~150 nm apart from the SiO<sub>2</sub> surface because the intensity is too weak to extract from the tail of the TO<sub>1</sub> peak.

Fig 2f shows the normalized intensity as a function of distance to the surface. The intensity of bulk mode TO<sub>3-bulk</sub> decreases to 1/3 at the surface within ~50nm. The intensity of the surface mode TO<sub>3-surface</sub> has the maximum value at the edge of surface and gradually decrease away from the edge (inset in Fig 2e). This can be understood by the geometry of thin foil structure, since the total intensity of the surface mode is contributed by the up surface, bottom surface, and edge surface. At the edge, all of them make significant contributions while far away from the edge only the up and bottom surface make contributions. The distribution of intensity of the TO<sub>3-surface</sub> in the vacuum can be described by the relativity-modified dielectric response theory[29], based on which the inelastic-scattering probability per unit energy loss E per unit length t for aloof-beam spectroscopy is[29]

$$\frac{dP}{dEdt} = \frac{4}{\pi} \frac{\alpha}{\hbar c \beta^2} \text{Im} \left( \frac{-1}{\varepsilon_{\text{SiO}_2}(E) + 1} \right) K_0 \left( \frac{2bE}{\gamma \hbar c \beta} \right) \quad (1)$$

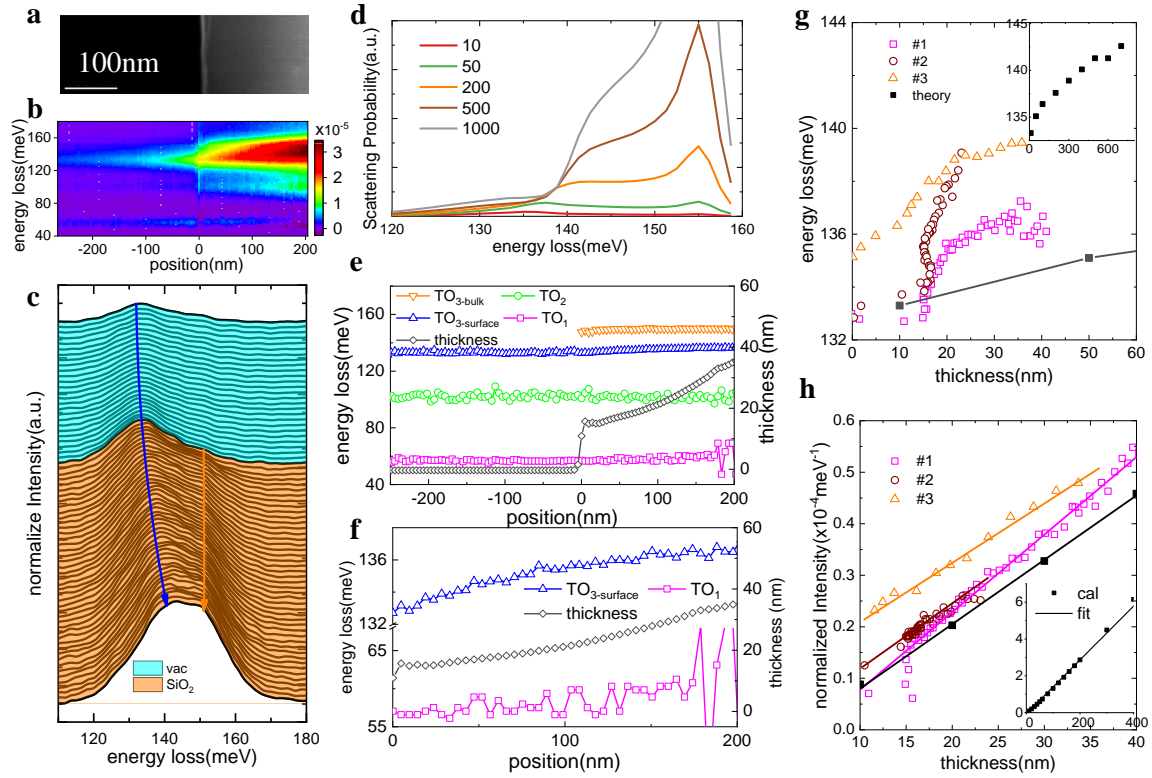


Fig 3. Effect of film thickness on the vibrational energy and intensity. (a) HAADF image of vacuum/ a-SiO<sub>2</sub> viewed in cross-section. (b) Two dimensional plots of normalized intensity for beam located in different region. The surface is labeled as zero, and negative distance denotes that the probing beam is in vacuum while positive distance denotes that the probing beam positioned in SiO<sub>2</sub>. Color represents the normalized intensity. (c) Selected line profile of the SiO<sub>2</sub> vibrational signal with 4.7 nm every stack. Orange region, beam located in SiO<sub>2</sub>; cyan region, beam located in vacuum. (d) Energy-loss functions of different z-thickness. (e) Energy of vibration modes (colored) and z-thickness (black) of SiO<sub>2</sub> slab as a function of the probe position. (f) Enlarged view of TO<sub>3-surface</sub> mode and TO<sub>1</sub> mode showing the peak shift depends on the film thickness. (g) Vibration energy of TO<sub>3-surface</sub> mode as a function of z-thickness of SiO<sub>2</sub> slab. Different color represents different data required from different samples and the black points are calculated from Kroger formula. (h) The intensity of TO<sub>3</sub> mode as a function of z-thickness of SiO<sub>2</sub> slab. Different color represents different data set from different samples and black point is calculation from Kroger formula.

where  $t$  is the specimen thickness,  $\alpha = 1/137$  is the fine-structure constant,  $\hbar$  is the reduced Planck constant,  $\beta = v/c$  is the ratio of beam velocity  $v$  to the speed of light  $c$ ,  $\gamma = (1 - \beta^2)^{-1/2}$  is the Lorentz factor,  $b$  is the impact parameter (the distance between the beam and the sample)

surface). The function  $K_0$  is the zero-order modified Bessel function of second kind, which represents the dependence of the vibration signal on the impact parameter  $b$ . The vibration intensity of surface mode  $TO_{1\text{-surface}}$  and  $TO_{3\text{-surface}}$  is very well described by equation (1). The Blue and Red solid line is the theoretical variation derived from Eq(1). The decay behavior can also roughly be fitted with the exponential function:  $I = I_0 \exp(-b/b_0)$  (ref.[11]). With this approximation, the decay distance is fitted to be  $\sim 400\text{nm}$  for  $TO_{1\text{-surface}}$ ,  $\sim 350\text{ nm}$  for  $TO_2$ , and  $\sim 250\text{ nm}$  for  $TO_{3\text{-surface}}$  (detailed data see Supporting Table 1). In bulk a-SiO<sub>2</sub>, the intensity of ‘bulk’ signal remains constant due to the nearly uniform thickness of the specimen.

When the thickness of specimen is in the order of  $v/\omega$  (where  $\omega$  is the frequency of vibration and  $v$  is electron beam velocity) or less, the coupling of upper and lower surfaces would give rise to symmetric and asymmetric guided modes[25]. Fig 3a, 3b, 3c shows the HAADF image, two-dimensional plots of normalized intensity, and selected line profiles of SiO<sub>2</sub> spectra (4.7 nm every step) with non-uniform thickness, respectively. As the beam is positioned from the edge to the inside, the energy of the  $TO_{3\text{-surface}}$  mode (blue line) shows significant blue-shift while the  $TO_{1\text{-surface}}$  shows smaller blue-shift, as shown in Fig 3f. We attribute the blue-shift to the reduced strength of coupling when  $z$ -thickness increases, as we will discuss below.

This energy shift behavior can also be interpreted by the thickness dependent energy-loss functions plotted in Fig 3d based on Kröger formula[25]. There are two important features. Firstly, the vibration energy of  $TO_{1\text{-surface}}$  and  $TO_{3\text{-surface}}$  modes increases as the specimen thickness increases, while the energy of  $TO_2$  mode almost remains unchanged. Consistently, the quantitative analysis in Fig 3e and Fig 3f confirms that the different vibration modes have different thickness dependent behavior. Specifically, the energy of the  $TO_{3\text{-surface}}$  mode at the edge is 132 meV and increases to 136 meV distanced  $\sim 200\text{ nm}$  from the edge. In Fig 3g, three data sets from different specimens and calculation based on Kröger formula further confirm that the energy of the  $TO_{3\text{-surface}}$  mode is very sensitive to SiO<sub>2</sub> thickness. This can be understood by the strong coupling between the upper and the lower surfaces, i.e., the coupling strength of the upper surface and the lower surface becomes weaker as  $z$ -thickness increases.

The vibration intensity also depends on the thickness of film. Compared to the  $TO_{3\text{-surface}}$  mode, the probability of  $TO_{3\text{-bulk}}$  mode decreases more quickly as the z-thickness decreases. The normalized intensity of  $TO_{3\text{-bulk}}$  mode is plotted as a function of  $SiO_2$  slab thickness for the three data sets. The calculated slopes are  $1.2 \times 10^{-6} meV^{-1} nm^{-1}$  for #1 data set,  $1.3 \times 10^{-6} meV^{-1} nm^{-1}$  for #2 data set, and  $1.5 \times 10^{-6} meV^{-1} nm^{-1}$  for #3 data set, which in good agreement with that derived from the calculated data  $1.5 \times 10^{-6} meV^{-1} nm^{-1}$  (as shown in the inset).

In the following we discuss the interface effect on the vibrational spectra. Fig 4a, 4b, 4c shows the atom resolution HAADF image of  $SiO_2/Si$  interface, selected line profiles of  $SiO_2$  spectra (4.7 nm every step) with non-uniform thickness, and two-dimensional plots of normalized intensity, respectively. Note that when the beam is located in the  $SiO_2$  side, the acquired signal is mixed with the signals of  $SiO_2$  (both surface mode and bulk mode) and  $SiO_2/Si$  interface mode. In principle, the pure signal of  $SiO_2/Si$  interface vibration mode can be obtained by placing the electron beam in the Si substrate for long-range Coulomb interaction, because the retardation effects mask any inherent vibrational signal of Si substrate[30]. Unfortunately, the signal in Si side is too weak to record even after very long acquisition. Fig 4d shows the energy loss function simulated near the  $SiO_2/Si$  interface, where two vibration modes (interface and bulk) were predicted to obtain. Similarly, we decompose the signal between 120 meV and 160 meV into two Gaussian peaks as the  $TO_{3\text{-bulk}}$  (from the bulk vibration with higher energy) and  $TO_{3\text{-surface+interface}}$  (from the interface vibration of  $SiO_2/Si$ , upper and lower surfaces of  $SiO_2$  with lower energy). Their energy and intensity are shown in Fig 4e and Fig 4f, respectively. Different color represents different sets of data. No significant energy shift of both modes is observed in Fig 4e. The intensity of both  $TO_{3\text{-bulk}}$  and  $TO_{3\text{-surface+interface}}$  modes drops steeply to zero within  $\sim 10$  nm of the a- $SiO_2/Si$  interface. The black solid line is the expected retarded signal intensity of  $TO_{3\text{-bulk}}$ , based on reference[31], which well describes the experiment data in the  $SiO_2$  side. The weak vibrational signal in the Si side may be due to surface oxide layers in Si substrate [30] or the diffused electron probe. The black dash line is the retarded signal intensity of  $TO_{3\text{-interface}}$ . The experimental intensity of  $TO_{3\text{-surface+interface}}$  is larger than that of the theoretical  $TO_{3\text{-interface}}$  due to the contribution of the

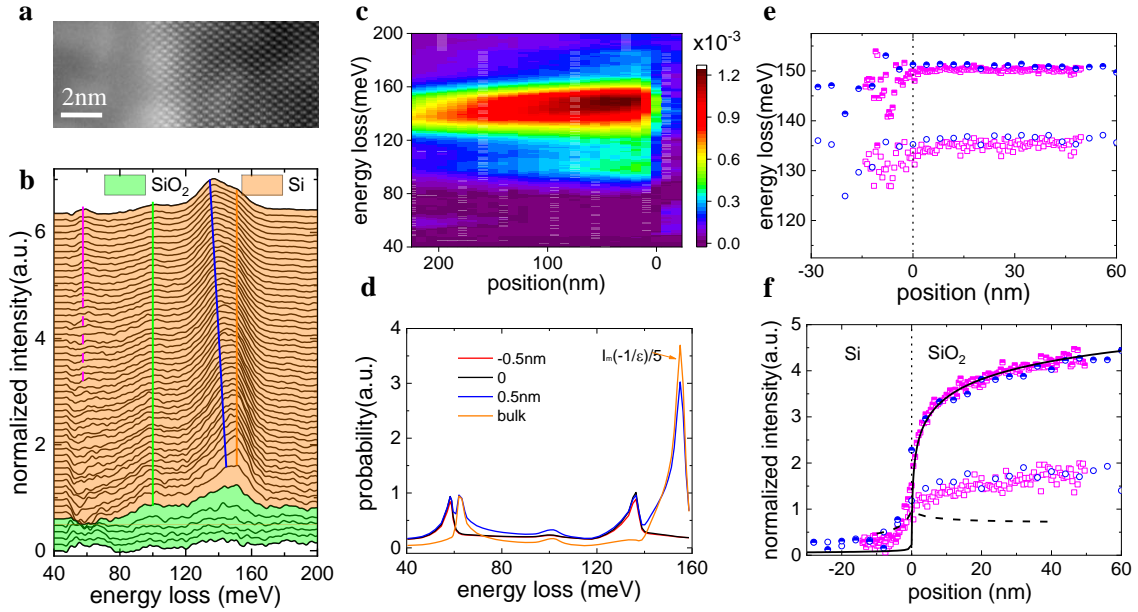


Fig 4. STEM Imaging, EELS spectra, vibrational energy and intensity as beam located in interface of SiO<sub>2</sub>/Si. (a) HAADF image of amorphous SiO<sub>2</sub>/Si viewed in cross-section. (b) Line profile of the SiO<sub>2</sub> vibrational signal with 0.78nm every stack. Orange region, beam located in a-SiO<sub>2</sub> side; green region, beam located in Si side. (c) Two dimensional plots of normalized intensity for beam located in different region. We labeled the interface at origin, and positive distance denotes that the probing beam is in SiO<sub>2</sub> while negative distance denotes that the probing beam is positioned in Si. Color represents the normalized intensity. (d) Simulated energy-loss function of beam located in different region. The probability of beam located in bulk is divided by 5 for a good view. (e) The energy of TO<sub>3</sub>-bulk mode and TO<sub>3</sub>-interface+surface mode as a function of the probe position; different color represents different sets of data; the open and the half up filled represent TO<sub>3</sub>-bulk mode and TO<sub>3</sub>-interface+surface mode, respectively. (f) Point: the intensity of TO<sub>3</sub>-bulk (TO<sub>3</sub>-interface+surface) mode as a function of the probe position with the same settings above; black solid (dash) line: theoretical retarded signal of TO<sub>3</sub>-bulk (TO<sub>3</sub>-interface) mode.

upper and the lower surface vibration TO<sub>3</sub>-surface of which the vibration energy is similar to that of interface vibration. For other vibration mode, because of the steep drop, it is rather hard to extract from the background signal.

Since the properties of the surface and interface of SiO<sub>2</sub> films can significantly influence the performance and stability of device[20,21], the miniaturization of MOSFET's and bipolar

transistors in the integrated circuits necessitates the investigation of these boundary conditions. The nanoscale measurements of vibration properties of the surface and interface presented above should be insightful for the device engineering via surface and interface treatments particularly for those devices with size below 14 nm.

## Conclusion

In summary, by using the monochromatic STEM-EELS in aberration corrected electron microscope, we investigate vibration behavior of surface and interface of SiO<sub>2</sub> film on Si substrate. With the improved energy resolution of sub-10 meV in the present study, three optical vibration modes of ~60 meV, ~103 meV and ~130–150 meV are recorded simultaneously. We find that all the surface modes have lower energy compared to the corresponding bulk modes, which is in good agreement with the local dielectric theory. Particularly, the energy of antisymmetric stretching mode is ~13 meV lower for the 60 nm-thick SiO<sub>2</sub> slab. The maximum intensity of surface mode occurs at the edge of surface and gradually decrease in the two sides. In the vacuum side, the intensity of surface vibration as a function of impact parameter accurately obey the zero-order modified Bessel function of the second kind[29] with typical decay distances ~400 nm for TO<sub>1-surface</sub>, ~350 nm for TO<sub>2</sub>, and ~250 nm for TO<sub>3-surface</sub>. Inside the SiO<sub>2</sub> film, the bulk mode has constant energy while the energy of surface mode strongly depends on the thickness. Approaching the interface of SiO<sub>2</sub>/Si, all the vibrational signal drops sharply within a few nanometers from the interface in SiO<sub>2</sub> side.

The highly sensitive of vibration properties to the surface, thickness and interface of SiO<sub>2</sub>/Si is expected to influence the electrical and thermal conductivities in a very complicate manner in MOSFET's and bipolar transistors. Therefore, our experimental measurements of local vibration properties SiO<sub>2</sub>/Si give useful clues for further understanding and controlling the properties of SiO<sub>2</sub>/Si heterostructure in future.

## Acknowledgement

The work was supported by the National Key R&D Program of China (grant numbers 2016YFA0300804 and 2016YFA0300903); the National Natural Science Foundation of China (Grant Nos. 51502007, 51672007), National Equipment Program of China (ZDYZ2015-1). We gratefully acknowledge the support from the National Program for Thousand Young Talents of China and “2011 Program” Peking-Tsinghua-IOP Collaborative Innovation Center of Quantum Matter. The authors acknowledge Electron Microscopy Laboratory in Peking University for the use of Cs corrected electron microscope.

## References

- [1] Ashcroft NW. Solid state physics. New York,: Holt, Rinehart and Winston; 1976.
- [2] Houchmandzadeh B, Lajzerowicz J, Salje E. Relaxations near surfaces and interfaces for first-, second- and third-neighbour interactions: theory and applications to polytypism. *J Phys Condens Matter* 1992;4:9779. doi:10.1088/0953-8984/4/49/006.
- [3] Xia F, Wang H, Xiao D, Dubey M, Ramasubramaniam A. Two-dimensional material nanophotonics. *Nat Photonics* 2014;8:899–907. doi:10.1038/nphoton.2014.271.
- [4] Maradudin AA, Oitmaa J. Longitudinal and transverse localized vibration modes. *Solid State Commun* 1969;7:1143–7. doi:10.1016/0038-1098(69)90503-1.
- [5] Electron Energy Loss Spectroscopy and Surface Vibrations. Elsevier; 1982. doi:10.1016/C2013-0-10894-X.
- [6] Zhang S, Guan J, Wang Y, Berlijn T, Johnston S, Jia X, et al. Lattice dynamics of ultrathin FeSe films on SrTiO<sub>3</sub>. *Phys Rev B* 2018;97:035408. doi:10.1103/PhysRevB.97.035408.
- [7] Griffiths PR, 1942-. Chemical infrared Fourier transform spectroscopy. Wiley; 1975.
- [8] Stuart B. Infrared Spectroscopy. Kirk-Othmer Encycl. Chem. Technol., American Cancer Society; 2005. doi:10.1002/0471238961.0914061810151405.a01.pub2.
- [9] Efremov EV, Ariese F, Gooijer C. Achievements in resonance Raman spectroscopy: Review of a technique with a distinct analytical chemistry potential. *Anal Chim Acta* 2008;606:119–34. doi:10.1016/j.aca.2007.11.006.
- [10] Steidtner J, Pettinger B. Tip-Enhanced Raman Spectroscopy and Microscopy on Single Dye Molecules with 15 nm Resolution. *Phys Rev Lett* 2008;100:236101.

doi:10.1103/PhysRevLett.100.236101.

- [11] Krivanek OL, Lovejoy TC, Dellby N, Aoki T, Carpenter RW, Rez P, et al. Vibrational spectroscopy in the electron microscope. *Nature* 2014;514:209–12. doi:10.1038/nature13870.
- [12] Lagos MJ, Trügler A, Hohenester U, Batson PE. Mapping vibrational surface and bulk modes in a single nanocube. *Nature* 2017;543:529–32. doi:10.1038/nature21699.
- [13] Rez P, Aoki T, March K, Gur D, Krivanek OL, Dellby N, et al. Damage-free vibrational spectroscopy of biological materials in the electron microscope. *Nat Commun* 2016;7:10945. doi:10.1038/ncomms10945.
- [14] Crozier PA, Aoki T, Liu Q. Detection of water and its derivatives on individual nanoparticles using vibrational electron energy-loss spectroscopy. *Ultramicroscopy* 2016;169:30–6. doi:10.1016/j.ultramic.2016.06.008.
- [15] Govyadinov AA, Konečná A, Chuvilin A, Vélez S, Dolado I, Nikitin AY, et al. Probing low-energy hyperbolic polaritons in van der Waals crystals with an electron microscope. *Nat Commun* 2017;8:95. doi:10.1038/s41467-017-00056-y.
- [16] Dwyer C, Aoki T, Rez P, Chang SLY, Lovejoy TC, Krivanek OL. Electron-Beam Mapping of Vibrational Modes with Nanometer Spatial Resolution. *Phys Rev Lett* 2016;117:256101. doi:10.1103/PhysRevLett.117.256101.
- [17] Hachtel JA, Lupini AR, Idrobo JC. Exploring the capabilities of monochromated electron energy loss spectroscopy in the infrared regime. *Sci Rep* 2018;8:5637. doi:10.1038/s41598-018-23805-5.
- [18] Hudak BM, Depner SW, Waetzig GR, Talapatra A, Arroyave R, Banerjee S, et al. Real-time atomistic observation of structural phase transformations in individual hafnia nanorods. *Nat Commun* 2017;8:15316. doi:10.1038/ncomms15316.
- [19] Idrobo JC, Lupini AR, Feng T, Unocic RR, Walden FS, Gardiner DS, et al. Temperature Measurement by a Nanoscale Electron Probe Using Energy Gain and Loss Spectroscopy. *Phys Rev Lett* 2018;120:095901. doi:10.1103/PhysRevLett.120.095901.
- [20] Nicollian EH. Electrical properties of the Si–SiO<sub>2</sub> interface and its influence on device performance and stability. *J Vac Sci Technol* 1977;14:1112–21. doi:10.1116/1.569343.
- [21] Kirton MJ, Uren MJ, Collins S, Schulz M, Karmann A, Scheffer K. Individual defects at the Si:SiO<sub>2</sub> interface. *Semicond Sci Technol* 1989;4:1116. doi:10.1088/0268-1242/4/12/013.
- [22] Tu Y, Tersoff J. Structure and Energetics of the Si-SiO<sub>2</sub> Interface. *Phys Rev Lett* 2000;84:4393–6.

doi:10.1103/PhysRevLett.84.4393.

- [23] Martinet C, Devine R a. B. Analysis of the vibrational mode spectra of amorphous SiO<sub>2</sub> films. *J Appl Phys* 1995;77:4343–8. doi:10.1063/1.359459.
- [24] Queeney KT, Weldon MK, Chang JP, Chabal YJ, Gurevich AB, Sapjeta J, et al. Infrared spectroscopic analysis of the Si/SiO<sub>2</sub> interface structure of thermally oxidized silicon. *J Appl Phys* 2000;87:1322–30. doi:10.1063/1.372017.
- [25] Kröger E. Berechnung der Energieverluste schneller Elektronen in dünnen Schichten mit Retardierung. *Z Für Phys Hadrons Nucl* 1968;216:115–35. doi:10.1007/BF01390952.
- [26] Moreau P, Brun N, Walsh CA, Colliex C, Howie A. Relativistic effects in electron-energy-loss-spectroscopy observations of the Si/SiO<sub>2</sub> interface plasmon peak. *Phys Rev B* 1997;56:6774–81. doi:10.1103/PhysRevB.56.6774.
- [27] Bates JB, Hendricks RW, Shaffer LB. Neutron irradiation effects and structure of noncrystalline SiO<sub>2</sub>. *J Chem Phys* 1974;61:4163–76. doi:10.1063/1.1681714.
- [28] Innocenzi P. Infrared spectroscopy of sol–gel derived silica-based films: a spectra-microstructure overview. *J Non-Cryst Solids* 2003;316:309–19. doi:10.1016/S0022-3093(02)01637-X.
- [29] Howie A. Surface reactions and excitations. *Ultramicroscopy* 1983;11:141–8. doi:10.1016/0304-3991(83)90229-2.
- [30] Venkatraman K, Rez P, March K, Crozier PA. The influence of surfaces and interfaces on high spatial resolution vibrational EELS from SiO<sub>2</sub>. *Microscopy* 2018;67:i14–23. doi:10.1093/jmicro/dfy003.
- [31] Garcia-Molina R, Gras-Marti A, Howie A, Ritchie RH. Retardation effects in the interaction of charged particle beams with bounded condensed media. *J Phys C Solid State Phys* 1985;18:5335. doi:10.1088/0022-3719/18/27/019.

# **Supplemental Material: Probing lattice vibration at surface and interface of SiO<sub>2</sub>/Si with nanometer resolution**

Yuehui Li<sup>1</sup>, Mei Wu<sup>1</sup>, Ning Li<sup>1,2</sup>, Yuanwei Sun<sup>1</sup>, Chenglong Shi<sup>3</sup>, Xuetao Zhu<sup>4</sup>, Jiandong Guo<sup>4</sup>, Dapeng Yu<sup>2,5,6</sup>, Peng Gao<sup>1,2,6\*</sup>

<sup>1</sup>International Center for Quantum Materials, School of Physics, Peking University, Beijing, 100871, China

<sup>2</sup>Electron Microscopy Laboratory, School of Physics, Peking University, Beijing, 100871, China

<sup>3</sup>Nion Co. 11511 NE 118Th Street, Kirkland, Washington State, 98034, USA

<sup>4</sup>Beijing National Laboratory for Condensed Matter Physics and Institute of Physics, Chinese Academy of Sciences, Beijing 100190, China

<sup>5</sup>Shenzhen Key Laboratory of Quantum Science and Engineering, Shenzhen 518055, China

<sup>6</sup>Collaborative Innovation Centre of Quantum Matter, Beijing 100871, China.

Y.H.L. and M.W. contributed equally to this work.

E-mails: [p-gao@pku.edu.cn](mailto:p-gao@pku.edu.cn)

**Data acquisition.** In our experiments, we used a Nion UltraSTEM200 microscope with both monochromator and the aberration corrector operating at 60kV. The beam convergence semi-angle was 15mrad and the collection semi-angle was 24.4 mrad with a 1 mm spectrometer entrance aperture. The typical energy resolution (half width of the full zero loss peak, ZLP) was 8meV, the probe beam current was ~5-10 pA and the dispersion of per channel was 0.47 meV. The typical dwell time was 100-200ms to obtain good signal-noise ratio spectra. The specimen studied in this work was 300 nm amorphous SiO<sub>2</sub> (a-SiO<sub>2</sub>) on Si substrate. We acquired single spectrum from different regions, line scan spectra, and map spectra to resolve the spatially dependent vibration properties.

**Calibration and background subtraction.** To correct the energy shift, we shifted the maximum point of ZLP to zero for unsaturated ZLP and shifted the centroid of two energies whose intensity was 5% lower than its peak value. To obtain more precise information from the spectra, we fitted the background with power law  $I(\Delta E) = A_0 \cdot \Delta E^{-r}$ . Note that generally, third order exponential provides a more accurate fit, but due to the high energy resolution (~8.3 meV), there is little benefit using the exponential[1].

**Theoretical analysis.** To quantitatively interpret the experiment results, calculation of the vibration response was performed. There are many theories and models based on classical dielectric response or quantum mechanical exploration to explain nanometer confined vibrations[2–5]. Here we do calculation mainly based on a semiclassical relativistic local dielectric model developed by E. KROGER[3], which considers the coupling of the upper and lower surface and gives rise to symmetric and asymmetric guided slab modes.

There are two reasons to choose Gaussian function to fit the peak rather than Lorentz function: (1), SiO<sub>2</sub> sample is amorphous; a dielectric function based on a modified Gaussian profile was used to reproduce the infrared reflectivity spectra of silicate glass[6]; (2), the probing function (ZLP) is approximated as Gaussian distribution. It should be noted that to get a better decomposition, a new background function was subtracted to make two sides of the TO<sub>3-bulk</sub> + TO<sub>3-surface</sub> signal approach zero, where two fitting region (105meV~115meV, 175meV~195meV) was chosen.

We calculate film thickness through plasmon peak, using formula:

$$t = \lambda \ln \frac{I_{tot}}{I_{ZLP}}$$

where,  $I_{tot}$  is the sum of all counts in a spectrum containing main plasmon signal,  $I_{ZLP}$  is the sum of zero loss peak,  $\lambda$  is the electron mean free path, whose detailed expression can be obtained from reference[7].

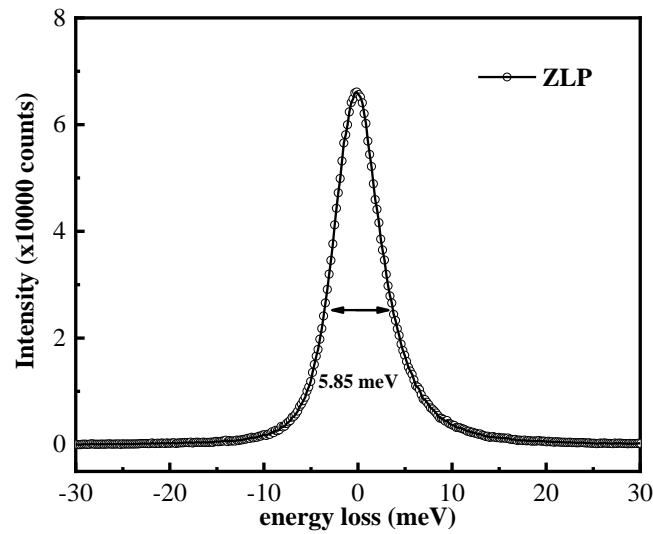
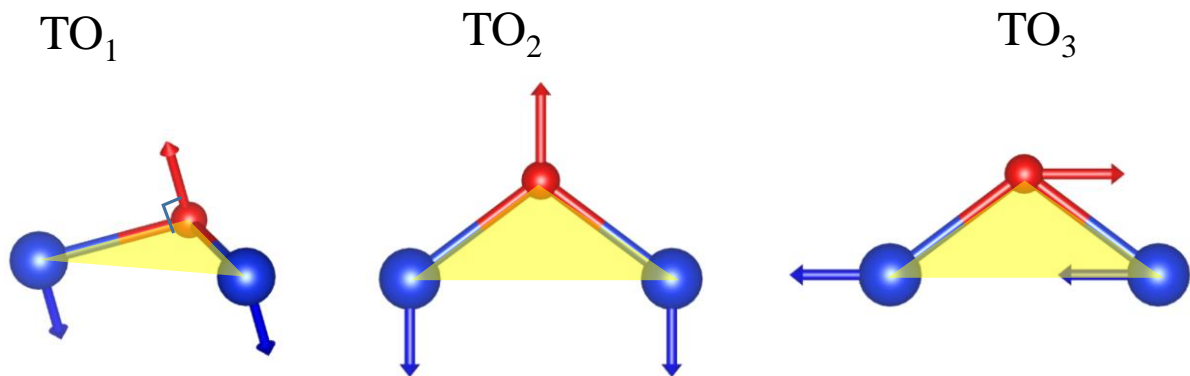
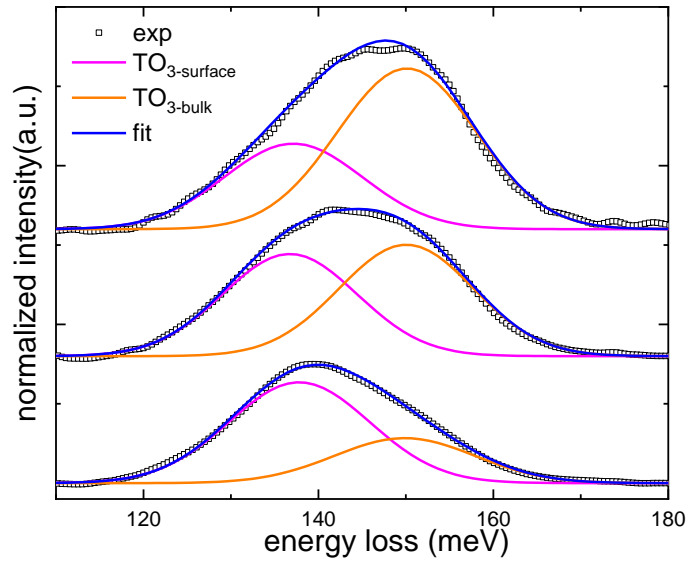


Fig S1: ~ 6meV FWHM zero loss peak



**Fig S2:** Sketch diagram of different vibration modes.  $TO_1$  mode, rocking motion perpendicular to Si-O-Si plane;  $TO_2$  mode, symmetric stretching motion along the bisector of the Si-O-Si bridging angle;  $TO_3$  mode, antisymmetric stretching motion parallel to the Si-Si line between the two bridged cations.



**Fig S3:** Gaussian function to fit the peak. black open square: experiment data; pink line:  $\text{TO}_{3\text{-surface}}$  mode component fitted; orange line:  $\text{TO}_{3\text{-bulk}}$  mode component fitted; blue line: sum of  $\text{TO}_{3\text{-surface}}$  mode component and  $\text{TO}_{3\text{-bulk}}$  mode component

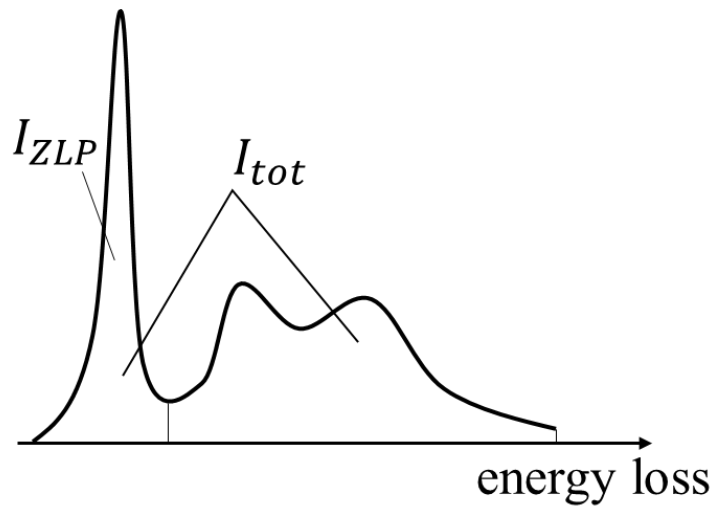


**Fig S4:** Sketch diagram of calculating thickness by log-ratio method.

	#1	#2	#3	#4
$\text{TO}_1$	415	380	394	
$\text{TO}_2$	357	338	333	353
$\text{TO}_3$	259	276	242	251

**Table 1.** decay constant  $b_0$  (nm) for different vibration modes. Different sets of data were fitted with exponential function  $I = I_0 \exp(-b/b_0)$ .

## Reference

- [1] Hachtel JA, Lupini AR, Idrobo JC. Exploring the capabilities of monochromated electron energy loss spectroscopy in the infrared regime. *Sci Rep* 2018;8:5637. doi:10.1038/s41598-018-23805-5.
- [2] Allen LJ, Brown HG, Findlay SD, Forbes BD. A quantum mechanical exploration of phonon energy-loss spectroscopy using electrons in the aloof beam geometry. *Microscopy* 2018;67:i24–9. doi:10.1093/jmicro/dfx038.
- [3] Kröger E. Berechnung der Energieverluste schneller Elektronen in dünnen Schichten mit Retardierung. *Z Für Phys Hadrons Nucl* 1968;216:115–35. doi:10.1007/BF01390952.
- [4] Howie A, Milne RH. Excitations at interfaces and small particles. *Ultramicroscopy* 1985;18:427–33. doi:10.1016/0304-3991(85)90161-5.
- [5] Forbes BD, Allen LJ. Modeling energy-loss spectra due to phonon excitation. *Phys Rev B* 2016;94:014110. doi:10.1103/PhysRevB.94.014110.
- [6] De Sousa Meneses D, Malki M, Echegut P. Structure and lattice dynamics of binary lead silicate glasses investigated by infrared spectroscopy. *J Non-Cryst Solids* 2006;352:769–76. doi:10.1016/j.jnoncrysol.2006.02.004.
- [7] Egerton RF. *Electron Energy-Loss Spectroscopy in the Electron Microscope*. 3rd ed. Springer US; 2011.